Broadband microwave signal generation with programmable chirp shapes via low-speed electronics-controlled phase-modulated optical loop

Weiqiang Lyu[1,2], Huan Tian[1,2], Zhenwei Fu[1,2], Lingjie Zhang[1,2], Zhen Zeng[1,2], Yaowen Zhang[1,2], Heping Li[1,2], Zhiyao Zhang[1,2],* & Yong Liu[1,2],*

[1] State Key Laboratory of Electronic Thin Films and Integrated Devices, School of Optoelectronic Science and Engineering, University of Electronic Science and Technology of China, Chengdu 610054, P. R. China
[2] Research Center for Microwave Photonics (RC-MWP), School of Optoelectronic Science and Engineering, University of Electronic Science and Technology of China, Chengdu 610054, P. R. China
*Corresponding author: Zhiyao Zhang (email: zhangzhiyao@uestc.edu.cn); Yong Liu (email: yongliu@uestc.edu.cn)

Broadband microwave signals with customized chirp shapes are highly captivating in practical applications. Compared with electronic technology, photonic solutions are superior in bandwidth, but suffer from flexible and rapid manipulation of chirp shape. Here, we demonstrate a novel concept for generating broadband microwave signals with programmable chirp shapes. It is realized on a simple fiber-optic platform involving a continuous-wave laser, a phase-modulated optical loop, low-speed electronics at MHz, and an optical coherent receiver. Microwave signals with bandwidths beyond tens of GHz, even up to hundreds of GHz, can be generated, where the chirp shape is identical to the low-frequency driving waveform of the phase-modulated optical loop. Besides, signal parameters, such as bandwidth, center frequency, and temporal duration, can be reconfigured in real time. In the experiment, highly-coherent microwave signals with various customized chirp shapes are generated, where the time resolution for programming the chirp shape is 649 ps. The center frequency and bandwidth tuning ranges exceed 21 GHz, and the temporal duration is tuned in the range of 9 ns to 180 ns.

Broadband chirped microwave signals with customized chirp shapes and reconfigurable parameters are widely used in military and civilian applications, such as modern radar systems[1, 2], monitoring of human vital signs[3-5], wireless communication[6, 7], and optical vector analysis[8]. For example, nonlinearly chirped microwave signals with well-designed chirp shapes are featured by low sidelobes after pulse compression, which is beneficial for enhancing false target detection dynamic range in radar systems. The general way of generating such microwave signals is to utilize high-speed electronics, e.g., arbitrary waveform generators (AWGs), which suffers from size, weight, and power (SWaP) problems. Besides, the attainable center frequency and bandwidth are restricted by the sampling rate of state-of-the-art digital-to-analog converters, which can hardly reach beyond tens of GHz at present.

In the past two decades, special attention has been paid to photonic solutions for broadband chirped microwave signal generation, thanks to the offered access to available bandwidths up to THz range[9-11]. Especially, with the rapid advancement of photonic integration technology, a large number of mature discrete photonic devices can be fabricated on chips, facilitating miniaturization, lightweighting and energy saving of photonic systems[12-14]. Hence, photonic solutions have the potential to solve the SWaP problem, and break the bandwidth limitation in chirped microwave signal generation. So far, numerous photonic approaches for generating broadband chirped microwave signals have been demonstrated, such as direct space-to-time mapping[15-17], spectral shaping followed by frequency-to-time mapping[18-24], and temporal pulse shaping[25-27]. Although much effort has been made to improve center frequency, bandwidth, and reconfigurability in the past, these techniques still suffer from low signal-to-noise ratio (SNR), small temporal duration, and limited time-bandwidth product (TBWP, generally < 100), which cannot meet the requirements of some practical applications. Spectral line-by-line shaping is a fine spectrum manipulation method for waveform synthesis, enabling SNR improvement and duration extension[28-32]. However, constrained by the number of the manipulable comb lines, this method also faces a great challenge in terms of TBWP (~ 100). Recently, frequency-shifting optical loop has been demonstrated to be an effective method to enhance TBWP beyond 1000[33-37]. Nevertheless, it can only generate linear frequency modulation or frequency-stepped microwave signals. To enlarge bandwidth, a feasible approach is to down-convert chirped optical signals to microwave domain via mixing them with a narrow-linewidth laser[38, 39]. The performance of the generated chirped microwave signals is mainly dependent on the initial chirped optical signals. As an alternative, optical modulation technique can be utilized to boost the center frequency and the bandwidth of the external chirped microwave signals[40-44]. However, a high-speed AWG is required to provide the initial chirped microwave signals.

In order to generate chirped microwave signals with large TBWPs, an optically-injected semiconductor laser operated in period-one oscillation state is a feasible solution[45-47]. Nevertheless, several stringent constraints on injection conditions must be satisfied to excite period-one oscillation[48], including polarization of the injection light, frequency detuning, and injection power, which increases system complexity and uncertainty. Another inventive approach is to employ Fourier domain mode locking (FDML) technique to break the limitation of mode building time in optoelectronic oscillators (OEOs)[49-53] or lasers[54], which is

capable of generating chirped microwave signals with TBWPs exceeding 10^5. The key component incorporated in OEOs or lasers is a high-quality-factor and fast-tuning filter with a tuning period or its multiple equal to the loop round-trip time. Based on this method, a fast frequency-scanning microwave or optical signal is produced after stable oscillation. However, for generating microwave signals with customized chirp shapes, a corresponding frequency-sweeping filter must be involved in the cavity, which increases the complexity of the photonic system to some extent. Besides, impeded by the existing techniques for building a fast and high-precision frequency-sweeping filter[49, 50], the actual chirp shape of the microwave signal from the FDML-based OEO/laser may severely deviate from its desired form. Otherwise, a chirped microwave signal with an expectant chirp shape is inevitably applied to construct an accurate frequency-scanning track of the filter[53], resulting in an augmentation in cost and SWaP.

In summary, a photonic solution for generating broadband microwave signals with precisely customized chirp shapes at low cost and small SWaP is still lacking. How to fully leverage the advantages of optoelectronic fusion to build a simple system with excellent SWaP performance for achieving this goal is still a concern in the scientific community.

Here, we demonstrate a novel concept for generating broadband microwave signals with customized chirp shapes on a simple fiber-optic platform. The platform involves a continuous-wave laser, a phase-modulated optical loop, low-speed electronics at MHz, and an optical coherent receiver. Based on this platform, highly-coherent chirped microwave signals with bandwidths beyond tens of GHz, even up to hundreds of GHz, can be generated. The most attractive characteristic of the proposed method lies in that the chirp shape of the generated microwave signal is identical to the low-frequency driving waveform of the phase-modulated optical loop. Hence, it offers an extremely simple way to manipulate the chirp shape of a high-frequency and broadband microwave signal through controlling the temporal waveform of a low-frequency driving signal via using low-speed electronics, e.g., a direct digital frequency synthesis (DDS) with a sampling rate at the level of tens of MSa/s and a vertical resolution beyond 20 bits. In addition, this method has excellent reconfigurability in bandwidth, center frequency, and temporal duration. In the experiment, microwave signals with various customized chirp shapes are generated. The time resolution for manipulating the chirp shape is 649 ps, exhibiting a robust ability to program the chirp shape. The tuning ranges of the center frequency and the bandwidth exceed 21 GHz, which can be easily enhanced to hundreds of GHz by using a photodetector with a larger operation bandwidth. In addition, the temporal duration is tuned in the range of 9 ns to 180 ns. Actually, it can be varied from tens of ps to tens of μs, which is determined by the period of the driving signal. The coherent time of the generated microwave signals is larger than 100 μs. Compared with the existing photonic solutions, the proposed method avoids the usage of fast and precise frequency-scanning filters/lasers, large dispersion mediums, and high-speed electronics. It fully leverages the huge bandwidth of the photonic technology, as well as the high-precision characteristics and the flexible programming ability of the electronic technology. Hence, the proposed concept paves a way to generate broadband microwave signals with user-definable chirp shapes, which can find applications in broadband radar systems, electronic warfare and spectroscopy.

Fig. 1. Photonic architecture for generating microwave waveforms with programmable chirp shapes. A phase-modulated optical fiber loop (round-trip time: τ_c) comprising an electro-optic phase modulator (PM), an optical bandpass filter (OBPF), an erbium-doped fiber amplifier (EDFA), and an optical coupler (OC), is utilized as an optical oscillator. A chirped optical waveform with a chirp shape identical to the low-frequency driving waveform from an AWG will be produced from the phase-modulated optical fiber loop. The output chirped optical signal is then down-converted to microwave domain by using an optical coherent detection device containing a 90° optical hybrid (OH) and a balanced photodetector (BPD), where a narrow-linewidth single-frequency laser from a laser diode (LD) acts as a local oscillator signal. The generated chirped microwave waveform is recorded by using an oscilloscope (OSC).

Results

Principle. Figure 1 shows the photonic architecture for generating microwave signals with programmable chirp shapes. The kernel of this scheme is a phase-modulated optical fiber loop with self-sustained oscillation, which is only seeded by amplified spontaneous emission (ASE) noise at each roundtrip. In the loop, an electro-optic phase modulator (PM) driven by a low-frequency signal from a low-speed AWG, achieves recirculating phase modulation of the self-sustained optical field. An optical bandpass filter (OBPF) is used to control the frequency span of the recirculating optical field. An erbium-doped fiber amplifier (EDFA) is utilized to supply the ASE noise and compensate for the loop loss. An optical coupler (OC) is employed to extract out a fraction of the optical field. The phase-modulated optical fiber loop is mainly described by two independent parameters: τ_c, the round-trip time of the loop (or $f_c = 1/\tau_c$, its free spectral range (FSR)), and f_s, the repetition frequency of the low-frequency driving signal (or $\tau_s = 1/f_s$, its period).

To generate chirped signals, the repetition frequency of the low-frequency driving signal slightly deviates from an integer multiple of the loop FSR. We define $\Delta f = f_s - kf_c \ll f_c$ as the frequency detuning, where k is a positive integer. Notice that Δf can be positive or negative. In this way, the optical field in the loop is phase-modulated by a time-delayed signal $s(t-n\tau_c)$ at the n-th roundtrip. A tiny time parameter can be denoted as $\tau_d = \tau_c - k\tau_s \ll \tau_c$. Since the driving signal is with a period of τ_s, the following equation is satisfied: $s(t-n\tau_c) = s(t-n\tau_d)$. Suppose that the driving signal $s(t)$ can be considered as a constant within a minuscule time span of τ_d, the recirculating phase modulation term experiencing n roundtrips, i.e., $\exp\left(im\sum_{l=1}^{l=n}s(t-l\tau_d)\right)$, can be approximatively represented in integral form as $\exp\left(\frac{im}{\tau_d}\int_{t-n\tau_d}^{t}s(u)du\right)$, where m is the modulation index of the PM. Besides, to ensure the self-sustained oscillation in the phase-modulated optical fiber loop only seeded by ASE noise $x_n(t)$, the net gain per roundtrip γ should be slightly larger than 1. As a result, the optical field output from the loop is the superposition of all the recirculating phase-modulated ASE noise, i.e., $E_0\sum_{n=1}^{n=N}\gamma^n x_n(t-n\tau_c)\exp\left(\frac{im}{\tau_d}\int_{t-n\tau_d}^{t}s(u)du\right)$, where E_0 and N represent the amplitude of the ASE noise seeded per roundtrip and the total number of the roundtrips, respectively. As detailed in the Methods, the output of the phase-modulated optical fiber loop can be mathematically derived as the product of a chirped term, i.e.,

$\exp\left(\frac{imf_cf_s}{\Delta f}\int_{0}^{t}s(u)du\right)$, and a single-frequency signal at q_0f_c, where q_0 is a positive integer. If the frequency detuning is set to be negative, i.e., $\Delta f < 0$, the output optical field is a chirped signal with a chirp shape identical to the temporal waveform of the low-frequency driving signal $s(t)$, a bandwidth of $|mf_cf_s / (\pi\Delta f)|$, a center frequency of q_0f_c, and a period of τ_s. Otherwise, i.e., $\Delta f > 0$, the chirp shape is identical to a reversed copy of $s(t)$, namely $-s(t)$. The center frequency q_0f_c is determined by the mode competition result between numerous intracavity modes, which can be tuned by adjusting the shape or the center frequency of the OBPF. Finally, by virtue of an optical coherent receiver including a 90° optical hybrid (OH) and a balanced photodetector (BPD), the chirped optical signal from the loop is mixed with a narrow-linewidth laser at f_{lo} to obtain a chirped microwave signal, where the influence of the intra-comb beating is eliminated. As shown in the chirp term of Eq. (14) in the Methods, the phases of the generated chirped microwave signals in different periods are identical to each other, which ensures mutual coherence of the generated signals. Actually, several nonideal factors will degrade the coherence of the generated chirped microwave signals, including the phase noise of the driving signals, the stability of the loop length and the optical gain, and the linewidth of the laser used for frequency down-conversion.

The chirp shape of the generated microwave signals can be customized through designing the temporal waveform of the low-frequency driving signal, which offers a low-cost and small SWaP access to obtain chirped microwave signals with a fast-reconfigurable chirp shape. Besides, for a certain loop length, its bandwidth, i.e., $|mf_cf_s / (\pi\Delta f)|$, is dependent on the modulation index, the repetition frequency of the driving signal, and the frequency detuning. In order to generate a microwave signal with a large bandwidth, the modulation index and the repetition frequency of the driving signal should be enlarged, and the frequency detuning should be reduced. A large modulation index can be achieved by the use of cascaded PMs. In addition, without the variation of the frequency detuning, the repetition frequency f_s can be manyfold enhanced to increase the bandwidth of the chirped microwave waveforms. Nevertheless, the period of the generated signal, i.e., $\tau_s = 1/f_s$, will be proportionally reduced, leading to a TBWP of $|mf_c / (\pi\Delta f)|$. Generally, the frequency detuning is a primary parameter used for controlling the bandwidth of the generated signals in the case of a fixed output period. Accordingly, the bandwidth of the OBPF should be
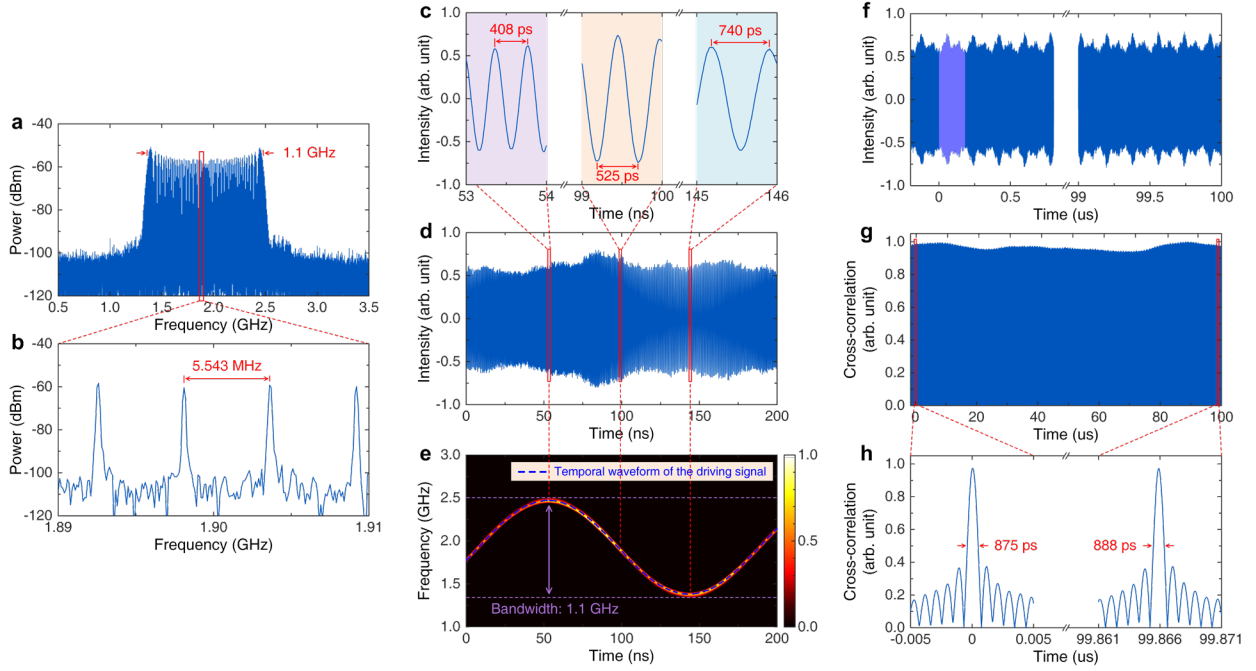
Fig. 2 Experimental results for generating sinusoidal chirped microwave signals. **a** Spectrum of the generated microwave signal within a frequency span of 3 GHz. **b** Spectrum detail within a frequency span of 20 MHz. **c** Temporal waveform details at the maximum, the intermediate, and the minimum instantaneous frequencies of the generated microwave signal. **d** Temporal waveform of the generated microwave signal within a temporal span of 200 ns. **e** Time-frequency distribution of the temporal waveform in **d**. **f** Microwave waveform within a temporal span of about 553 periods used for numerical calculation of the temporal cross-correlation trace. The reference waveform is plotted in light purple. **g** Calculated cross-correlation trace between the reference waveform and the whole waveform plotted in **c**. **h** Two magnified cross-correlation traces with a null time delay and a delay of about 100 μs, respectively.

adjusted to match the output bandwidth. In most cases, the ratio of the loop FSR to the frequency detuning, i.e., $f_c/\Delta f$, can reach several hundred or even one thousand, depending on the quality factor of the optical fiber loop. Besides, commercial PMs can easily meet the injection microwave power requirement for reaching a modulation index of 2π. As a result, the TBWP of the generated chirped microwave signals can easily reach beyond several hundred, or even up to a few thousand, on the fiber-optic platform. The center frequency of the generated chirped microwave signal is determined by the difference between the center frequency of the chirped optical signal and the frequency of the local oscillator laser, i.e., $|q_0 f_c - f_{lo}|$. The temporal duration of the generated chirped microwave signal, namely its period, is equal to the period of the driving signal. It can be easily tuned in the range of the loop round-trip time through varying the repetition frequency of the driving signal. A larger temporal duration can be realized by extending the length of the phase-modulated optical fiber loop. Since the period of the generated chirped signal deviates from a multiple of the loop round-trip time by τ_d, the instantaneous frequency of the optical field after each roundtrip will hop to ensure the continuity of the chirp shape. Hence, the instantaneous frequency of the optical energy in any section of the optical loop will travel along the chirp shape after recirculating a round-trip number of $\tau_s/\tau_d = f_c/\Delta f$, as exhibited in the Videos and detailed in the Supplementary Note 3.

The prominent advantage of the proposed scheme lies in that only a low-frequency electrical signal $s(t)$ is required, without the need of other high-speed electronics, to manipulate the chirp shape of the generated high-frequency and broadband chirped microwave signals. As a reference, the frequency span of $s(t)$ commonly ranges from f_s to a few multiples of f_s, resulting in a bandwidth amplification of about $|mf_c / (\pi\Delta f)|$. From another

perspective, the proposed scheme generates an equivalent group-velocity dispersion (GVD) to time-stretch an unchirped signal to be a chirped one. Unlike the GVD provided by a spool of optical fiber, the equivalent GVD varies in the frequency span of the output bandwidth, and can be controlled by $s(t)$. For a typical case of linearly chirped signal generation, the equivalent GVD, i.e., the slope of the linear group delay as a function of radial frequency, is calculated as $|\Delta f/(2mf_c f_s^2)|$, which corresponds to propagating through a spool of standard single-mode fiber with a length larger than thousands of kilometers.

Experimental results. Several experiments based on the fiber-optic platform in Fig. 1 are implemented to exhibit the capabilities of the proposed concept for generating chirped microwave signals with tunable center frequency, controllable output bandwidth, variable temporal duration, and customized chirp shape.

Firstly, we characterize the performance of the proposed scheme in generating microwave signals with sinusoidal chirp shapes. The FSR of the phase-modulated optical fiber loop is measured to be 5.563 MHz, corresponding to a round-trip time of 179.8 ns. The driving signal is a single-tone microwave signal, i.e., a sinusoidal signal, with a repetition frequency of 5.543 MHz, from an AWG (RIGOL). Hence, the frequency detuning is 0.02 MHz. Besides, the modulation index is set to be its maximum achievable value of 0.72π, which is limited by the half-wave voltage of the available PM (EOSPACE) and the output power of the AWG. The optical gain provided by an EDFA is finely adjusted to guarantee that the net gain in the loop is slightly larger than 1. In this way, the bandwidth of the chirped optical signal from the phase-modulated optical fiber loop is calculated to be about 1.1 GHz according to Eq. (8) in the Methods. To ensure self-sustained oscillation of the chirped optical signal in the phase-
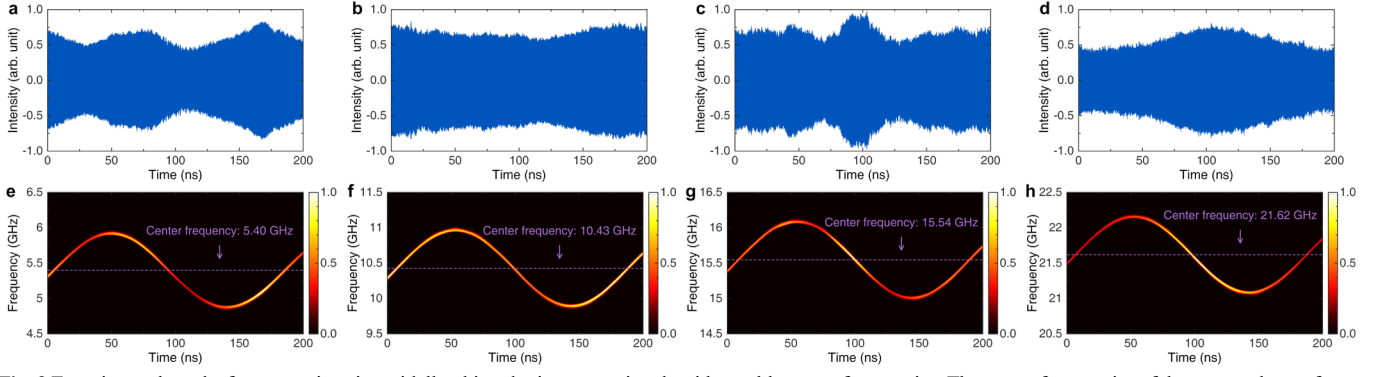
Fig. 3 Experimental results for generating sinusoidally-chirped microwave signals with tunable center frequencies. The center frequencies of the temporal waveforms in **a-d** are equal to 5.40 GHz, 10.43 GHz, 15.54 GHz, and 21.62 GHz, respectively. **e-h** Corresponding time-frequency distributions of the temporal waveforms in **a-d**, calculated by Wigner-Ville distribution.
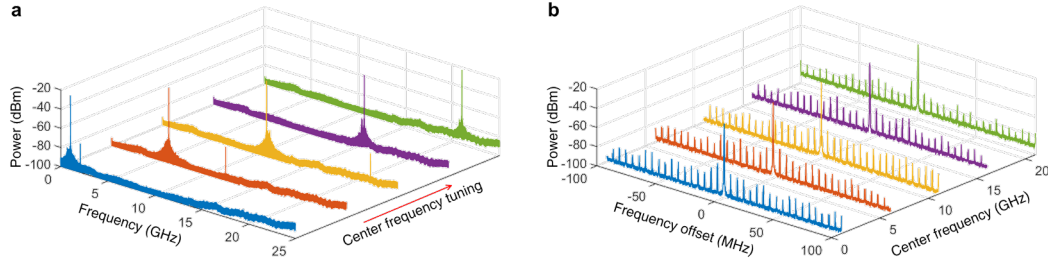

Fig. 4 Experimental results for generating single-tone microwave signals with tunable center frequencies when the phase-modulated optical fiber loop is operated at free-running state. **a** Frequency tuning of the output single-tone microwave signal by varying the frequency of the local oscillator laser. **b** Zoom-in views of **a** at the vicinity of the center frequencies.

modulated optical fiber loop, the bandwidth of the OBPF is tuned to match the output bandwidth and filter out the out-of-band ASE noise. The more accurate the bandwidth of the OBPF is, the smaller amount of the chirped signals with an identical chirp shape and an adjacent frequency interval of f_c will be generated in the initial stage, as expressed in the Methods. As a result, fewer chirped optical signals will participate in mode competition, leading to a stabler oscillation and a more excellent phase noise performance. Then, with the help of a customized optical coherent receiver, a continuous-wave laser (NKT Photonics) with a linewidth less than 100 Hz is used as the local oscillator signal to down-convert the generated chirped optical signal to microwave domain. Finally, a high-speed real-time oscilloscope (Keysight) with a sampling rate of 256 GSa/s is employed to capture the temporal waveforms of the generated chirped microwave signals. Figure 2a shows the measured spectrum of the generated chirped microwave signal. As expected, the output bandwidth is about 1.1 GHz. The spectrum detail within a span of 20 MHz is displayed in Fig. 2b. The frequency interval between neighboring teeth, i.e. the repetition frequency of the generated chirped microwave signal, is 5.543 MHz, which is identical to the repetition frequency of the driving signal. Figure 2c exhibits the temporal waveform details at the maximum, the intermediate, and the minimum instantaneous frequencies of the generated chirped microwave signal. Figure 2d presents the temporal waveform of the generated chirped microwave signal. The period of the generated chirped microwave signal is identical to that of the driving signal, namely 180.4 ns. The flat temporal envelope makes it more attractive in practical applications, such as radar systems, since a high SNR can be obtained when a flat chirped waveform is used for pulse compression. The corresponding time-frequency distribution is obtained by computing the Wigner-Ville distribution of the measured waveform, as shown in Fig. 2e. The frequency span of

the time-frequency distribution curve is 1.1 GHz. Hence, the TBWP of the generated chirped microwave waveform is equal to about 200, limited by the low-quality factor of the optical fiber loop and the relatively small modulation index. Besides, the temporal waveform of the low-frequency driving signal, i.e., a single-tone signal, is also presented as the blue dashed line in Fig. 2e to compare it with the chirp shape of the generated microwave signal. For the sake of comparison, the temporal waveform is proportionally scaled to match the amplitude of the time-frequency distribution curve. As consistent with the theoretical derivation, the chirp shape of the generated microwave signal is identical to the temporal waveform of the driving signal. Actually, the electro-optic phase modulation is a linear process, ensuring a linearly scaled conversion from the temporal waveform of the driving signal to the chirp shape of the generated microwave waveform. Thus, the proposed scheme provides a low-cost and small SWaP solution for manipulating the time-frequency distribution of the generated chirped microwave signals. To demonstrate the mutual coherence of the generated chirped microwave signal, a 100-µs-long temporal waveform is recorded, corresponding to about 553 periods, as shown in Fig. 2f. Thereinto, a single-period waveform as depicted in light purple in Fig. 2f is extracted out from the whole waveform to act as a reference for calculating the temporal cross-correlation trace. The whole cross-correlation trace presented in Fig. 2g has a relatively flat profile. The two cross-correlation peaks at the null time delay and the delay of about 100 µs, as displayed in Fig. 2h, show consistent shapes, without attenuation and broadening, indicating that the generated chirped microwave signal is with a high degree of coherence. The pulse width of the cross-correlation peaks is about $\tau = 875$ ps. Hence, the pulse compression ratio, defined as the ratio of the temporal period of the generated chirped signal to τ, is calculated to be about 206, which is almost equal to the TBWP.
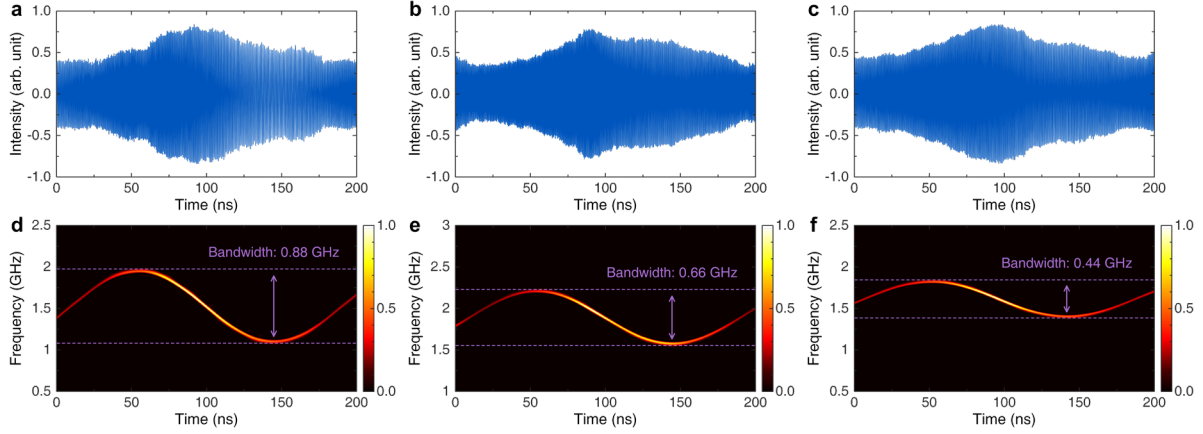
Fig. 5 Experimental results for generating sinusoidally-chirped microwave signals with controllable bandwidths through varying the modulation index. The modulation indices applied for generating the temporal waveforms in **a-c** are equal to 0.570π, 0.428π, and 0.285π, respectively. **d-f** Corresponding time-frequency distributions of the temporal waveforms in **a-c**, calculated by Wigner-Ville distribution.
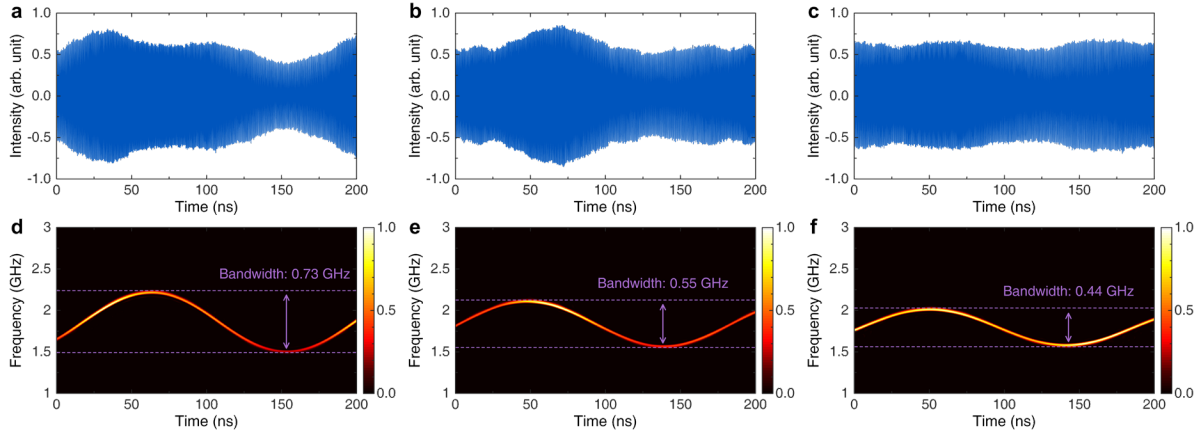

Fig. 6 Experimental results for generating sinusoidally-chirped microwave signals with controllable bandwidths through varying the frequency detuning. The frequency detuning employed for generating the temporal waveforms in **a-c** are equal to 0.03 MHz, 0.04 MHz, and 0.05 MHz, respectively. **d-f** Corresponding time-frequency distributions of the temporal waveforms in **a-c**, calculated by Wigner-Ville distribution.

Fig. 7 Experimental results for generating sinusoidally-chirped microwave signals with controllable bandwidths through varying the repetition frequency of the driving signal. The repetition frequencies of the driving signals used for generating the temporal waveforms in **a-c** are equal to 27.793 MHz, 55.610 MHz, and 111.240 MHz, respectively. **d-f** Corresponding time-frequency distributions of the temporal waveforms in **a-c**, calculated by Wigner-Ville distribution.
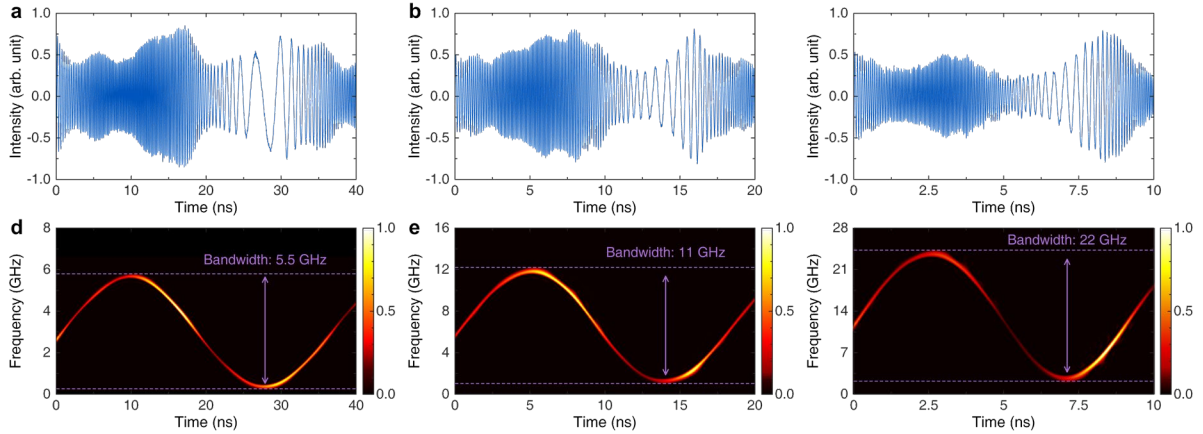
This result also indicates that the generated chirped microwave signal has a high coherence.

Then, we demonstrate the ability of the proposed scheme to tune the center frequency of the generated chirped microwave signals. The center frequency is tuned through varying the frequency of the continuous-wave laser used as the local oscillator signal, where the center frequency of the chirped microwave signals is equal to the difference between the center frequency of the chirped optical signals and the frequency of the continuous-wave laser. Figure 3 shows the generated sinusoidally-chirped microwave signals with an identical bandwidth but with different center frequencies of 5.40 GHz, 10.43 GHz, 15.54 GHz and 21.62
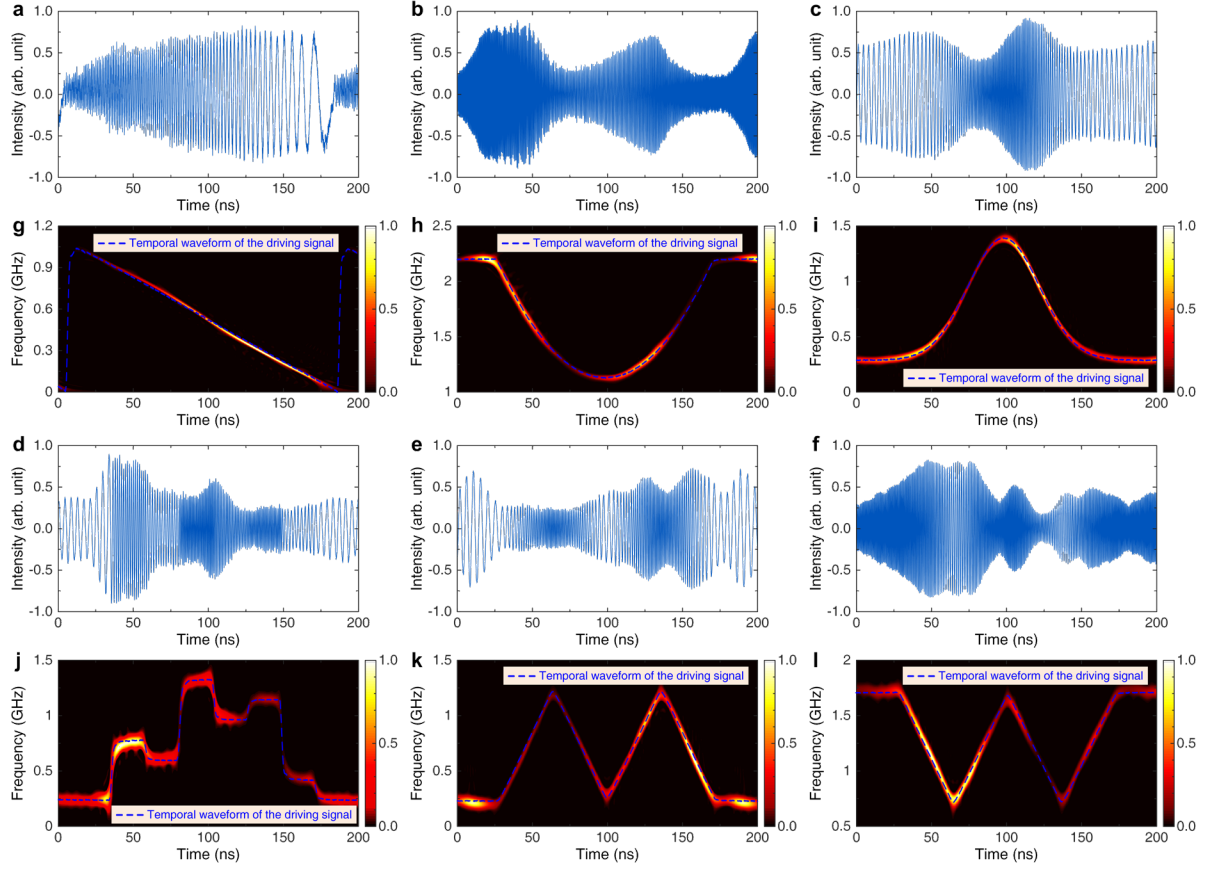
Fig. 8 Experimental results for generating microwave signals with customized chirp shapes. The generated microwave signals with temporal waveforms shown in **a-f** are a linearly chirped signal, a quadratically chirped signal, a gaussian-pulse-shaped chirped signal, a Costas-coded frequency-hopping signal with a 6-bit Costas coding sequence of [3 2 6 4 5 1], a 'M'-shaped chirped signal, and a 'W'-shaped chirped signal, respectively. **g-l** Corresponding time-frequency distributions of the temporal waveforms in **a-f**, calculated by Wigner-Ville distribution.

GHz, respectively. The distinction between the temporal envelopes of the four chirped microwave signals is induced by the frequency response difference of the electronic detection devices in different frequency bands. To further investigate the center frequency tuning process, the optical fiber loop is operated at the free-running state, i.e., without recirculating phase modulation, to observe the frequency tuning of the generated single-tone microwave signals. Figure 4a displays the spectra of the generated single-tone microwave signals. Thereinto, the 2nd-order harmonics are produced by the nonlinear photoelectric conversion due to the large injecting optical power of the BPD. The center frequency can be tuned in a frequency span beyond 21 GHz, which is limited by the operation bandwidth of the optical coherent receiver. The zoom-in views of Fig. 4a at the vicinity of the center frequencies are shown in Fig. 4b. Owing to the mode competition, the output of the free-running optical fiber loop only contains a single-tone signal, and has a side-mode suppression ratio larger than 40 dB, which gives evidence for supporting mode competition deduction in the Methods. The center frequency of the generated chirped microwave signals can also be tuned by adjusting the center frequency of the OBPF.

The bandwidth of the generated chirped microwave signal is another controllable parameter in the proposed scheme. According to Eq. (8) in the Methods, without varying the length of the phase-modulated optical fiber loop, i.e., under a fixed f_c, the output bandwidth depends on three parameters, including the modulation index, the frequency detuning, and the repetition

frequency of the driving signal. Figure 5 shows the temporal waveforms and the corresponding time-frequency distributions of the generated sinusoidally-chirped microwave signals with different bandwidths, where the modulation indices are equal to 0.570π, 0.428π, and 0.285π, respectively. As expected, the bandwidth ratio of the generated chirped microwave signals is equal to 4:3:2, i.e., 0.88 GHz : 0.66 GHz : 0.44 GHz. The similar envelopes of the temporal waveforms shown in Fig. 5a-c indicate that the increase of the modulation index makes no distortion on the output temporal waveform. The output bandwidth can also be controlled through varying the frequency detuning, as displayed in Fig. 6. The output bandwidth is inversely proportional to the frequency detuning, which is consistent with Eq. (8) in the Methods. Besides, a larger frequency detuning leads to a smaller amount of $f_c/\Delta f$, which corresponds to fewer roundtrips for the intracavity optical field to travel along the chirp shape. It means that, for a phase-modulated optical fiber loop with a certain quality factor, the larger the frequency detuning is, the more times the intracavity optical field will periodically travel along the chirp shape. Owing to the mode competition, the more times the optical field periodically travels along the chirp shape in the time-frequency plane, the flatter the generated temporal waveform will be. As exhibited in Fig. 6, the generated temporal waveform gets flatter as the frequency detuning increases. Without the variation of the frequency detuning, the repetition frequency of the driving signal can be increased to enhance the output bandwidth. Figure 7 shows the generated temporal waveforms and the corresponding

time-frequency distributions when the repetition frequencies of the driving signals are increased to five times, ten times, and twenty times of that applied in Fig. 2. Correspondingly, the output bandwidths are proportionally increased to 5.5 GHz, 11 GHz, and 22 GHz, respectively. Here, the maximum output bandwidth is limited by the operation bandwidth of the optical coherent receiver used in the experiment. Besides, the temporal durations of the chirped microwave signals are proportionally decreased to 36 ns, 18 ns, and 9 ns due to the diminution in modulation periods.

The most remarkable advantage provided by the proposed scheme lies in that the chirp shape of the generated microwave signal is identical to the temporal waveform of the driving signal. In other words, the chirp shape of the generated microwave signal can be arbitrarily customized through designing the temporal waveform of the driving signal, without other complex operations. Besides, the bandwidth ratio of the generated chirped microwave signal to the driving signal is generally larger than several hundred, indicating that the chirp shape of a high-frequency and broadband microwave signal can be manipulated by a low-frequency waveform. Figure 8 exhibits the temporal waveforms and the time-frequency distributions of the generated chirped microwave signals with various customized chirp shapes. The temporal waveforms of the driving signals are also presented as blue dashed lines in Fig. 8. Thereinto, all the chirp shapes of the generated microwave signals are identical to the temporal waveforms of the driving signals, which shows a robust manipulation ability of the chirp shape. In addition, the output bandwidth is fixed for generating microwave signals with any chirp shape. It is noteworthy that the minimum time span for customizing the chirp shape is equal to τ_d since the driving signal is assumed as a constant in a time span of τ_d. In other words, the time resolution of the proposed scheme for programming the chirp shape is equal to τ_d. Generally, the time resolution represented by $\tau_d = (\Delta f/f_c)\tau_s$ is less than a hundredth, or even a thousandth of the period of the generated microwave signal on the fiber-optic platform. Here, the ratio $f_c/\Delta f$ and the period of the generated microwave signals are equal to 278 and 180.4 ns, respectively, corresponding to a time resolution as small as 649 ps. To realize a smaller time resolution, an oscillation loop with a high-quality factor must be employed, such as OEOs and optical microresonators.

Discussion

In summary, we have proposed a novel concept for generating broadband chirped microwave signals with programmable chirp shapes by using a simple architecture. Both theoretical analysis and experiments are implemented to verify the feasibility of the proposed method. It is based on a phase-modulated optical fiber loop with self-sustained oscillation, where the modulation period slightly deviates from the loop round-trip time. Proof-of-concept experiments are carried out on a fiber-optic platform involving a continuous-wave laser, a phase-modulated optical fiber loop, low-speed electronics at MHz, and an optical coherent receiver, avoiding the use of pulse shapers, frequency-scanning filters, large dispersion mediums, or high-frequency electronics in the vast majority of the reported approaches so far. Hence, the proposed concept for generating broadband chirped microwave signals with customized chirp shapes offers a remarkable improvement in terms of system cost, structural complexity, and SWaP performance, which makes it attractive for practical application. Besides, the proposed concept can also be applied in other platforms such as OEOs and optical microresonators, where

more distinguished performance can be expected since a higher quality factor can be provided.

The generated chirped microwave signals can be flexibly reconfigured in center frequency, bandwidth, time duration, and chirp shape. The tuning range of the center frequency and the bandwidth reported here are exclusively limited by the available bandwidth of the optical coherent receiver, which can be easily enhanced to exceed hundreds of GHz through using a photodetector with a larger operation bandwidth, e.g., a uni-traveling-carrier photodiode (UTC-PD). The temporal duration of the generated chirped signal is identical to the period of the driving signal, and its maximum value is limited by the loop round-trip time. Hence, chirped microwave signals with a temporal duration in the μs range can be easily generated in a long loop. Accordingly, generation of shorter chirped microwave waveforms can be achieved through simply increasing the repetition frequency of the driving signals, without varying the loop length. The most extraordinary feature offered by the proposed scheme lies in that the chirp shape of the generated broadband microwave signal is identical to the temporal waveform of the low-frequency driving signal, which gives us an extremely simple way to manipulate the chirp shape through designing the temporal waveform of a low-frequency signal. The cross-correlation trace of the output chirped microwave signals indicates a highly mutual coherence in a time span exceeding 100 μs. This characteristic is greatly prominent for many practical applications, e.g., pulse compression radars. Such a large coherent time enables the detection range of the radar systems to exceed tens of kilometers. The TBWP of about 200 in the experiment is restricted by the limited modulation index and the relatively-low quality factor of the optical fiber loop. With the help of the cascaded phase modulation structure and the photonic integration technology, the TBWP of the generated chirped microwave signals can be enhanced by several orders of magnitude. The demonstrated performance and the predictable potential development of the proposed scheme show an excellent advancement in generating chirped microwave signals that are suitable for numerous applications such as broadband radar systems, electronic warfare and spectroscopy.

Methods

Output from the proposed photonic architecture. Considering a phase-modulated optical fiber loop with a round-trip time of τ_c (or a free spectral range of $f_c = 1/\tau_c$) and driven by a direct current (DC)-free normalized waveform $s(t)$ with a repetition frequency of f_s (or a period of $\tau_s = 1/f_s$), the output optical field after stable oscillation can be expressed as

$$E_{out}(t) = E_0 \sum_{n=1}^{N} \gamma^n x_n(t - n\tau_c) \exp\left(im \sum_{l=1}^{n} s(t - l\tau_c) \right), \qquad (1)$$

where E_0 and $x_n(t)$ are the amplitude and the normalized temporal waveform of the ASE noise added by the EDFA at the roundtrip of N-n+1, respectively. Thereinto, N is the total number of the roundtrips. The net gain per roundtrip γ should be set to be a little larger than 1 to ensure self-sustained oscillation of the phase-modulated optical fiber loop. The modulation index $m = \pi V/V_\pi$ is determined by the driving voltage V and the half-wave voltage V_π of the PM. In the proposed scheme, there is a tiny frequency detuning $\Delta f \ll f_c$ between the repetition frequency of the driving signal and the oscillation frequency of the phase-modulated optical fiber loop, i.e., $\Delta f = f_s$ - kf_c (k is a positive integer), where Δf can be positive or negative. Defining a time parameter $\tau_d = \tau_c$ - $k\tau_s = \Delta f / f_s f_c$, then $s(t - l\tau_c) = s(t - l\tau_c + kl\tau_s) = s(t - l\tau_d)$ since τ_s is the period of $s(t)$. τ_d is quite small compared with the period of $s(t)$. Hence, the driving signal $s(t)$ can be approximatively regarded as a constant within a time span of τ_d. As a result, $s(t - l\tau_d)$ can be expressed in integral form as

$$s(t - l\tau_d) = s(t - l\tau_d) \times 1 \approx \frac{1}{\tau_d} \int_{t - l\tau_d}^{t - (l-1)\tau_d} s(u)\, du. \qquad (2)$$

Similarly, the summation of $s(t - l\tau_d)$ from $l = 1$ to $l = n$ can be written as

$$\sum_{l=1}^{n} s(t - l\tau_d) \approx \frac{1}{\tau_d} \int_{t-n\tau_d}^{t} s(u) du. \tag{3}$$

A primitive function of $s(t)$ in the interval of $t \geq 0$ can be written as

$$y(t) = \int_{0}^{t} s(u) du. \tag{4}$$

Through substituting Eq. (3) and Eq. (4) into Eq. (1), we can obtain

$$E_{out}(t) \approx E_0 \sum_{n=1}^{N} \gamma^n x_n(t - n\tau_c) \exp\left(\frac{im}{\tau_d}\left(y(t) - y(t - n\tau_d)\right)\right). \tag{5}$$

Defining a new function $p(t) = \exp\left(-\frac{im}{\tau_d} y(t)\right)$ and its Fourier transform

$P(f) = \int p(t) \exp(-i2\pi f t) dt$, a simplified form of Eq. (5) is given as

$$E_{out}(t) \approx p^{-1}(t) E_0 \sum_{n=1}^{N} \gamma^n x_n(t - n\tau_c) p(t - n\tau_d). \tag{6}$$

Since $s(t)$ is DC-free and with a period of τ_s, $y(t)$ and $p(t)$ are also periodic signals with a period of τ_s, leading to an equality transformation: $p(t - n\tau_d) = p(t - n\tau_d - kn\tau_s) = p(t - n\tau_c)$. For the sake of clarity, the output optical field is divided into two parts as $E_{out}(t) \approx p^{-1}(t)v(t)$, where $v(t)$ is defined as

$$v(t) = E_0 \sum_{n=1}^{N} \gamma^n x_n(t - n\tau_c) p(t - n\tau_c). \tag{7}$$

For the first part $p^{-1}(t)$, its instantaneous frequency is calculated as

$$f(t) = -\frac{1}{2\pi} \frac{d}{dt}\left(\frac{m}{\tau_d} y(t)\right) = -\frac{mf_c f_s}{2\pi\Delta f} s(t). \tag{8}$$

Obviously, through setting the frequency detuning Δf to be negative, the chirp shape $f(t)$ of the first part is consistent with a scaled form of the driving signal $s(t)$, and its frequency span is from $mf_c f_s / (2\pi\Delta f)$ to $-mf_c f_s / (2\pi\Delta f)$. Besides, the period of the generated chirped signal is identical to that of the driving signal rather than the round-trip time of the optical fiber loop, leading to a TBWP of $|mf_c / (\pi\Delta f)|$. In order to achieve a large TBWP, it is required to maximize the modulation index and the ratio of the loop FSR to the frequency detuning. As for the second part $v(t)$, it can be simplified in the frequency domain by using the multiplication property of the Fourier transform

$$V(f) = E_0 \sum_{n=1}^{N} \gamma^n \int x_n(t - n\tau_c) p(t - n\tau_c) \exp(-i2\pi f t) dt$$
$$= \frac{E_0}{2\pi} \sum_{n=1}^{N} \gamma^n \left[X_n(f)\exp(-i2n\pi f\tau_c)\right] * \left[P(f)\exp(-i2n\pi f\tau_c)\right] \tag{9}$$
$$= \frac{E_0}{2\pi} \sum_{n=1}^{N} \gamma^n \left[X_n(f) * P(f)\right] \exp(-i2n\pi f\tau_c),$$

where $X_n(f) = \int x_n(t)\exp(-i2\pi f t)dt$ is the Fourier transform of $x_n(t)$. The power spectrum of the ASE noise added in each roundtrip can be approximatively considered to be identical owing to the fixed driving electrical current of the EDFA. Hence, we can replace $X_n(f)$ by the power spectrum $X_N(f)$ of the additional ASE noise in the first roundtrip. Then, simple mathematics of Eq. (9) leads to

$$V(f) = \frac{E_0}{2\pi} \left[X_N(f) * P(f)\right] \frac{\gamma \exp(-i2\pi f\tau_c) - \gamma^{N+1}\exp(-i2(N+1)\pi f\tau_c)}{1 - \gamma \exp(-i2\pi f\tau_c)}. \tag{10}$$

In general, the roundtrip number N is greater than 10^5, resulting in $\gamma^{N+1} \gg \gamma$. Then, Equation (10) can be simplified as

$$V(f) = \frac{E_0}{2\pi} \left[X_N(f) * P(f)\right] \frac{\gamma^{N+1}\exp(-i2(N+1)\pi f\tau_c)}{\gamma \exp(-i2\pi f\tau_c) - 1}. \tag{11}$$

For simplicity, $D(f)$ is utilized to represent the result of $[X_N(f)*P(f)]$ in Eq. (11). $p(t)$ is a periodic signal with a period of τ_s, which means that its Fourier

transform $P(f)$ is a multiple comb signal with an adjacent comb interval of f_s. In addition, the power spectrum $X_N(f)$ of the additional ASE noise in each roundtrip is with a bandwidth equal to the bandwidth of the OBPF. Thus, $D(f)$ is a broadband signal covering the whole bandwidth of the OBPF. Since γ is extremely close to 1, Equation (11) takes the maximum values at $f = qf_c$ (q is a positive integer), and its value at the frequency slightly deviated from qf_c is quite small compared with that at $f = qf_c$. On the other hand, the frequencies qf_c are also the oscillation modes in the phase-modulated optical fiber loop. Hence, $V(f)$ represents an optical frequency comb with frequencies of qf_c. Combined with the first part $p^{-1}(t)$, it means that the output optical field is the superposition of multiple customized chirped signals with an adjacent frequency interval of f_c. It is worth mentioning that there is a slight difference between the round-trip time of the phase-modulated optical fiber loop and an integral multiple of the output chirped signal period, i.e., $|\tau_c - k\tau_s|$. Consequently, the instantaneous frequency of the optical energy in any position of the phase-modulated optical fiber loop will travel along the customized chirp shape as it recirculates in the loop, as shown in the Videos. In our configuration, the bandwidth of the OBPF is set to match that of the desired chirped signal. As a result, only the generated chirped signals unfiltered by the OBPF in the traveling process can be remained in the phase-modulated optical fiber loop, which immensely decreases the number of the chirped signal replicas. Moreover, the mode competition between these chirped signal replicas will further reduce its number. Ultimately, only a single customized chirped signal will exist in the phase-modulated optical fiber loop after tens of thousands of roundtrips. Then, Eq. (11) is evolved as

$$V(f) = \frac{E_0}{2\pi} D(q_0 f_c) \frac{\gamma^{N+1}}{\gamma - 1} \delta(f + q_0 f_c), \tag{12}$$

where $\delta(f)$ is the unit impulse function. Through performing the inverse Fourier transform of $V(f)$ and combining it with the first part $p^{-1}(t)$, the final output optical field of the phase-modulated optical fiber loop can be mathematically expressed as

$$E_{out}(t) \approx \frac{E_0 \gamma^{N+1}}{4\pi^2(\gamma - 1)} D(q_0 f_c) \exp\left(-i2\pi\left(q_0 f_c t - \frac{mf_c f_s}{2\pi\Delta f}\int_0^t s(u)du\right)\right). \tag{13}$$

Equation (13) reveals that the output optical field is a chirped signal with a center frequency of $q_0 f_c$, a chirp shape identical to the temporal waveform of the driving signal $s(t)$, and a bandwidth of $mf_c f_s / (\pi\Delta f)$. To obtain a chirped microwave signal, the output optical chirped signal is combined with a continuous-wave laser $E_{lo}\exp(-i2\pi f_{lo}t)$ by the use of an optical coherent receiver to down-convert it to microwave domain. The photocurrent corresponding to the generated chirped microwave signal can be written as

$$I_{out}(t) \approx \frac{RE_0 E_{lo}\gamma^{N+1}}{4\pi^2(\gamma - 1)} D(q_0 f_c) \cos\left(2\pi(q_0 f_c - f_{lo})t - \frac{mf_c f_s}{\Delta f}\int_0^t s(u)du\right), \tag{14}$$

where R is the responsivity of the optical coherent receiver. Equation (14) indicates that the output from the proposed photonic architecture is a chirped microwave signal with a center frequency equal to $q_0 f_c - f_{lo}$, a time-frequency distribution identical to the temporal waveform of the driving signal $s(t)$, and a bandwidth of $mf_c f_s / (\pi\Delta f)$.

Data availability
The data that support the findings of this study are available from the corresponding author upon reasonable request.

References
1. Barton, D. K. *Radar System Analysis and Modeling* (Artech House, Norwood, MA, USA, 2005).
2. Richards, M. A. *Fundamentals of Radar Signal Processing* (McGraw-Hill, Hamilton, USA, 2005).
3. Wang, G. C., Muñoz-Ferreras, J. M., Gu, C. Z., Li, C. Z. & Gómez-García, R. Application of Linear-Frequency-Modulated Continuous-Wave (LFMCW) Radars for Tracking of Vital Signs. *IEEE Trans. Microw. Theory Tech.* **62**, 1387-1399 (2015).
4. Alizadeh, M., Shaker, G., De Almeida, J. C. M., Morita, P. P. & Safavi-Naeini, S. Remote Monitoring of Human Vital Signs Using mm-Wave FMCW Radar. *IEEE Access* **7**, 54958-54968 (2019).
5. Wang, W. S. et al. Wideband Gain Enhancement of MIMO Antenna and Its Application in FMCW Radar Sensor Integrated With CMOS-Based Transceiver

Chip for Human Respiratory Monitoring. *IEEE Trans. Antennas Propag.* **71**, 318-329 (2023).

6. De Oliveira, L. G. et al. Joint Radar-Communication Systems: Modulation Schemes and System Design. *IEEE Trans. Microw. Theory Tech.* **70**, 1521-1551 (2022).

7. Nie, H. J., Zhang, F. Z., Yang, Y. & Pan, S. L. Photonics-based integrated communication and radar system. In *International Topical Meeting on Microwave Photonics (MWP)*, Ottawa, Canada, 42-45 (2019).

8. Pan, S. L. & Xue, M. Ultrahigh-Resolution Optical Vector Analysis Based on Optical Single-Sideband Modulation. *J. Lightwave Technol.* **35**, 836-845 (2017).

9. Cundiff, S. T. & Weiner, A. M. Optical arbitrary waveform generation. *Nat. Photonics* **4**, 760-766 (2010).

10. Yao, J. P. Photonic generation of microwave arbitrary waveforms. *Opt. Commun.* **284**, 3723-3736 (2011).

11. Rashidinejad, A., Li, Y. H. & Weiner, A. M. Recent Advances in Programmable Photonic-Assisted Ultrabroadband Radio-Frequency Arbitrary Waveform Generation. *IEEE J. Quantum Electron.* **52**, 0600117 (2016).

12. Marpaung, D., Yao, J. P. & Capmany, J. Integrated microwave photonics. *Nat. Photonics* **13**, 80-90 (2019).

13. Bogaerts, W. et al. Programmable photonic circuits. *Nature* **586**, 207-216 (2020).

14. Zhu, D. et al. Integrated photonics on thin-film lithium niobate. *Adv. Opt. Photonics* **13**, 242-352 (2021).

15. McKinney, J. D., Seo, D. S., Leaird, D. E. & Weiner, A. M. Photonically Assisted Generation of Arbitrary Millimeter-Wave and Microwave Electromagnetic Waveforms via Direct Space-to-Time Optical Pulse Shaping. *J. Lightwave Technol.* **21**, 3020-3028 (2003).

16. Wang, C. & Yao, J. P. Large Time-Bandwidth Product Microwave Arbitrary Waveform Generation Using a Spatially Discrete Chirped Fiber Bragg Grating. *J. Lightwave Technol.* **28**, 1652-1660 (2010).

17. Bazargani, H. P. & Azaña, J. Optical pulse shaping based on discrete space-to-time mapping in cascaded co-directional couplers. *Opt. Express* **23**, 23450-23461 (2015).

18. Chou, J., Han, Y. & Jalali, B. Adaptive RF-photonic arbitrary waveform generator. *IEEE Photonics Technol. Lett.* **15**, 581-583 (2003).

19. Ashrafi, R., Park, Y. & Azaña, J. Fiber-Based Photonic Generation of High-Frequency Microwave Pulses With Reconfigurable Linear Chirp Control. *IEEE Trans. Microw. Theory Tech.* **58**, 3312-3319 (2010).

20. Dezfooliyan, A. & Weiner, A. M. Photonic synthesis of high fidelity microwave arbitrary waveforms using near field frequency to time mapping. *Opt. Express* **21**, 22974-22987 (2013).

21. Rashidinejad, A. & Weiner, A. M. Photonic Radio-Frequency Arbitrary Waveform Generation With Maximal Time-Bandwidth Product Capability. *J. Lightwave Technol.* **32**, 3383-3393 (2014).

22. Khan, M. H. et al. Ultrabroad-bandwidth arbitrary radiofrequency waveform generation with a silicon photonic chip-based spectral shaper. *Nat. Photonics* **4**, 117-120 (2010).

23. Li, Y. H. et al. Photonic generation of W-band arbitrary waveforms with high time-bandwidth products enabling 3.9 mm range resolution. *Optica* **1**, 446-454 (2014).

24. Wang, J. et al. Reconfigurable radio-frequency arbitrary waveforms synthesized in a silicon photonic chip. *Nat. Commun.* **6**, 5957 (2015).

25. Chi, H. & Yao, J. Symmetrical waveform generation based on temporal pulse shaping using amplitude-only modulator. *Electron. Lett.* **43**, 415-417 (2007).

26. Thomas, S. et al. Programmable fiber-based picosecond optical pulse shaper using time-domain binary phase-only linear filtering. *Opt. Lett.* **34**, 545-547 (2009).

27. Li, M., Wang, C., Li, W. Z. & Yao, J. P. An Unbalanced Temporal Pulse-Shaping System for Chirped Microwave Waveform Generation. *IEEE Trans. Microw. Theory Tech.* **58**, 2968-2975 (2010).

28. Jiang, Z., Huang, C. B., Leaird, D. E. & Weiner, A. M. Optical arbitrary waveform processing of more than 100 spectral comb lines. *Nat. Photonics* **1**, 463-467 (2007).

29. Huang, C. B., Jiang, Z., Leaird, D. E., Caraquitena, J. & Weiner, A. M. Spectral line-by-line shaping for optical and microwave arbitrary waveform generations. *Laser Photon. Rev.* **2**, 227-248 (2008).

30. Supradeepa, V. R. et al. Comb-based radiofrequency photonic filters with rapid tunability and high selectivity. *Nat. Photonics* **6**, 186-194 (2012).

31. Metcalf, A. J. et al. Integrated line-by-line optical pulse shaper for high-fidelity and rapidly reconfigurable RF-filtering. *Opt. Express* **24**, 23925-23940 (2016).

32. Schnébelin, C., Azaña, J. & de Chatellus, H. G. Programmable broadband optical field spectral shaping with megahertz resolution using a simple frequency shifting loop. *Nat. Commun.* **10**, 4654 (2019).

33. de Chatellus, H. G., Cortés, L. R., Schnébelin, C., Burla, M. & Azaña, J. Reconfigurable photonic generation of broadband chirped waveforms using a single CW laser and low-frequency electronics. *Nat. Commun.* **9**, 2438 (2018).

34. Zhang, Y. M., Liu, C., Shao, K. L., Li, Z. Y. & Pan, S. L. Multioctave and reconfigurable frequency-stepped radar waveform generation based on an optical frequency shifting loop. *Opt. Lett.* **45**, 2038-2041 (2020).

35. Yin, Z. Q., Zhang, X. P., Liu, C. Y., Zeng, H. N. & Li, W. Z. Wideband reconfigurable signal generation based on recirculating frequency-shifting using an optoelectronic loop. *Opt. Express* **29**, 28643-28651 (2021).

36. Lyu, Y. J. et al. Photonic Generation of Highly-Linear Ultra-Wideband Stepped-Frequency Microwave Signals With Up to $6 \cdot 10^6$ Time-Bandwidth Product. *J. Lightwave Technol.* **40**, 1036-1042 (2022).

37. Ma, C., Wang, X. C., Yang, Y., Ding, Z. Y. & Pan, S. L. Coherent stepped-frequency waveform generation based on recirculating microwave photonic frequency conversion. *Opt. Lett.* **48**, 4985-4988 (2023).

38. Gao, H. B. et al. A simple photonic generation of linearly chirped microwave pulse with large time-bandwidth product and high compression ratio. *Opt. Express* **21**, 23107-23115 (2013).

39. Wun, J. M. et al. Photonic chirped radio-frequency generator with ultra-fast sweeping rate and ultra-wide sweeping range. *Opt. Express* **21**, 11475-11481 (2013).

40. Kanno, A. & Kawanishi, T. Broadband Frequency-Modulated Continuous-Wave Signal Generation by Optical Modulation Technique. *J. Lightwave Technol.* **32**, 3566-3572 (2014).

41. Li, W., Wang, W. T., Sun, W. H., Wang, L. X. & Zhu, N. H. Photonic generation of arbitrarily phase-modulated microwave signals based on a single DDMZM. *Opt. Express* **22**, 7446-7457 (2014).

42. Zhang, K. et al. Photonic generation of multi-frequency dual-chirp microwave waveform with multiplying bandwidth. *Results Phys.* **13**, 102226 (2019).

43. Wang, L. et al. Photonic generation of multiband and multi-format microwave signals based on a single modulator. *Opt. Lett.* **45**, 6190-6193 (2020).

44. Li, P. et al. Photonic approach for the generation of switchable down-, up-, and dual-chirped linear frequency-modulated microwave signals. *Opt. Lett.* **45**, 1990-1993 (2020).

45. Zhou, P., Zhang, F. Z., Guo, Q. S. & Pan, S. L. Linearly chirped microwave waveform generation with large time time-bandwidth product by optically injected semiconductor laser. *Opt. Express* **24**, 18460-18467 (2016).

46. Zhou, P., Zhang, F. Z., Guo, Q. S., Li, S. M. & Pan, S. L. Reconfigurable Radar Waveform Generation Based on an Optically Injected Semiconductor Laser. *IEEE J. Sel. Top. Quantum Electron.* **23**, 1801109 (2017).

47. Zhou, P., Chen, H., Li, N. Q., Zhang, R. H. & Pan, S. L. Photonic generation of tunable dual-chirp microwave waveforms using a dual-beam optically injected semiconductor laser. *Opt. Lett.* **45**, 1342-1345 (2020).

48. Chan, S. C., Hwang, S. K. & Liu, J. M. Period-one oscillation for photonic microwave transmission using an optically injected semiconductor laser. *Opt. Lett.* **15**, 14921-14935 (2007).

49. Hao, T. F. et al. Breaking the limitation of mode building time in an optoelectronic oscillator. *Nat. Commun.* **9**, 1839 (2018).

50. Hao, T. F., Tang, J., Li, W., Zhu, N. H. & Li, M. Tunable Fourier Domain Mode-Locked Optoelectronic Oscillator Using Stimulated Brillouin Scattering. *IEEE Photonics Technol. Lett.* **30**, 1842-1845 (2018).

51. Hao, T. F. et al. Dual-chirp Fourier domain mode-locked optoelectronic oscillator. *Opt. Lett.* **44**, 1912-1915 (2019).

52. Hao, T. F., Tang, J., Li, W., Zhu, N. H. & Li, M. Harmonically Fourier Domain Mode-Locked Optoelectronic Oscillator. *IEEE Photonics Technol. Lett.* **31**, 427-430 (2019).

53. Zeng, Z. et al. Frequency-definable linearly chirped microwave waveform generation by a Fourier domain mode locking optoelectronic oscillator based on stimulated Brillouin scattering. *Opt. Express* **28**, 13861-13870 (2020).

54. Tang, J. et al. Hybrid Fourier-domain mode-locked laser for ultra-wideband linearly chirped microwave waveform generation. *Nat. Commun.* **11**, 3814 (2020).

Acknowledgements

Author contribution

W.Q.L. and Z.Y.Z. conceived the project. W.Q.L. carried out the experiments. H.T. and Z.W.F. performed the numerical simulations. L.J.Z., Z.Z., Y.W.Z. and H.P.L. conducted the theoretical analysis. W.Q.L., Z.Y.Z., and Y.L. carried out the data analysis. W.Q.L. wrote the manuscript with contributions from all authors. Y.L. finalized the paper. Z.Y.Z and Y.L. supervised the project.

Competing interests

The authors declare no competing interests.